Ruan, Yinlan; Afshar Vahid, Shahraam; Monro, Tanya Mary
Efficient excitation of surface plasmons in metal nanorods using large longitudinal component of high index nano fibers, *Optics Express*, 2011; 19(14):13464-13479

Efficient excitation of surface plasmons in metal nanorods using large longitudinal component of high index nano fibers

Yinlan Ruan,* Shahraam Afshar V., and Tanya M. Monro

Institute for Photonics & Advanced Sensing, School of Chemistry & Physics, The University of Adelaide, North Terrace, Adelaide, 5005, Australia

Yinlan.ruan@.adelaide.edu.au

Abstract: We report theoretical calculations of the mode fields of high index lead silicate and silicon nano fibers, and show that their strong longitudinal component enables efficient excitation of surface plasmons within a silver nanorod placed at the fiber tip. An excitation efficiency 1600 times higher than that of the standard single mode fibers has been achieved using a 350nm diameter silicon fiber at 1.1μm wavelength, while a factor of 640 times higher efficiency is achieved for a 400nm diameter lead silicate F2 glass fiber. The strong localized field emerging from the end of the rod serves as a nano-scale source with adjustable beam width, and such sources offer a new approach to high-resolution microscopy, particle manipulation and sensing.

OCIS codes: (060.2310) Fiber optics; (240.6680) Optics at surfaces.

References and links

1. A. Hartschuh, "Tip-enhanced near-field optical microscopy," Angew. Chem. Int. Ed. Engl. **47**(43), 8178–8191 (2008).
2. H. Eghlidi, K. G. Lee, X. W. Chen, S. Gotzinger, and V. Sandoghdar, "Resolution and enhancement in nanoantenna-based fluorescence microscopy," Nano Lett. **9**(12), 4007–4011 (2009).
3. G. Volpe, R. Quidant, G. Badenes, and D. Petrov, "Surface plasmon radiation forces," Phys. Rev. Lett. **96**(23), 238101 (2006).
4. T. Kalkbrenner, U. Hakanson, A. Schadle, S. Burger, C. Henkel, and V. Sandoghdar, "Optical microscopy via spectral modifications of a nanoantenna," Phys. Rev. Lett. **95**(20), 200801 (2005).
5. L. Novotny, R. X. Bian, and X. S. Xie, "Theory of nanometric optical tweezers," Phys. Rev. Lett. **79**(4), 645–648 (1997).
6. A. Drezet, M. J. Nasse, S. Huant, and J. C. Woehl, "The optical near-field of an aperture tip," Europhys. Lett. **66**(1), 41–47 (2004).
7. T. H. Taminiau, R. J. Moerland, F. B. Segerink, L. Kuipers, and N. F. van Hulst, "λ/4 resonance of an optical monopole antenna probed by single molecule fluorescence," Nano Lett. **7**(1), 28–33 (2007).
8. http://www.ntmdt-tips.com/catalog/snom/red/products/MF003.html.
9. T. Kalkbrenner, M. Ramstein, J. Mlynek, and V. Sandoghdar, "A single gold particle as a probe for apertureless scanning near-field optical microscopy," J. Microsc. **202**(1), 72–76 (2001).
10. P. Bharadwaj, P. Anger, and L. Novotny, "Nanoplasmonic enhancement of single-molecule fluorescence," Nanotechnology **18**(4), 044017 (2007).
11. S. Afshar V and T. M. Monro, "A full vectorial model for pulse propagation in emerging waveguides with subwavelength structures part I: Kerr nonlinearity," Opt. Express **17**(4), 2298–2318 (2009), http://www.opticsinfobase.org/oe/abstract.cfm?URI=oe-17-4-2298.
12. H. Ebendorff-Heidepriem and T. M. Monro, "Extrusion of complex preforms for microstructured optical fibers," Opt. Express **15**(23), 15086–15092 (2007), http://www.opticsinfobase.org/oe/abstract.cfm?URI=oe-15-23-15086.
13. H. Ebendorff-Heidepriem, S. C. Warren-Smith, and T. M. Monro, "Suspended nanowires: fabrication, design and characterization of fibers with nanoscale cores," Opt. Express **17**(4), 2646–2657 (2009), http://www.opticsinfobase.org/oe/abstract.cfm?URI=oe-17-4-2646.
14. S. C. Warren-Smith, H. Ebendorff-Heidepriem, T. C. Foo, R. Moore, C. Davis, and T. M. Monro, "Exposed-core microstructured optical fibers for real-time fluorescence sensing," Opt. Express **17**(21), 18533–18542 (2009), http://www.opticsinfobase.org/oe/abstract.cfm?URI=oe-17-21-18533.

#145479 - $15.00 USD Received 6 Apr 2011; revised 6 Jun 2011; accepted 13 Jun 2011; published 28 Jun 2011

15. P. Mehta, N. Healy, N. F. Baril, P. J. A. Sazio, J. V. Badding, and A. C. Peacock, "Nonlinear transmission properties of hydrogenated amorphous silicon core optical fibers," Opt. Express **18**(16), 16826–16831 (2010), http://www.opticsinfobase.org/oe/abstract.cfm?URI=oe-18-16-16826.
16. Y. Ruan, H. Ebendorff-Heidepriem, S. Afshar, and T. M. Monro, "Light confinement within nanoholes in nanostructured optical fibers," Opt. Express 1**8**, 26018–26026 (2010), http://www.opticsinfobase.org/oe/abstract.cfm?URI=oe-18-25-26018.
17. A. W. Snyder and J. D. Love, *Optical Waveguide Theory* (Chapman &Hall, London, UK, 1983).
18. N. Harris, M. J. Ford, P. Mulvaney, and M. B. Cortie, "Tunable infrared absorption by metal nanoparticles: the case for gold rods and shells," Gold Bull. **41**(1), 5–14 (2008).
19. E. D. Palik, *Handbook of Optical Constants of Solids* (Academic Press, New Yor, 1985).
20. T. J. Norman, Jr., C. D. Grant, D. Magana, J. Z. Zhang, J. Liu, D. Cao, F. Bridges, and A. Van Buuren, "Near infrared optical absorption of gold nanoparticle aggregates," J. Phys. Chem. B **106**(28), 7005–7012 (2002).
21. http://www.corning.com/docs/specialtymaterials/pisheets/pi101.pdf.
22. L. Novotny, M. R. Beversluis, K. S. Youngworth, and T. G. Brown, "Longitudinal field modes probed by single molecules," Phys. Rev. Lett. **86**(23), 5251–5254 (2001).
23. H. Ishitobi, I. Nakamura, N. Hayazawa, Z. Sekkat, and S. Kawata, "Orientational imaging of single molecules by using azimuthal and radial polarizations," J. Phys. Chem. B **114**(8), 2565–2571 (2010).
24. http://www.illuminex.biz.
25. S. Ramachandran, P. Kristensen, and M. F. Yan, "Generation and propagation of radially polarized beams in optical fibers," Opt. Lett. **34**(16), 2525–2527 (2009).
26. S. Nie and S. R. Emory, "Probing single molecules and single nanoparticles by surface-enhanced Raman scattering," Science **275**(5303), 1102–1106 (1997).
27. R. P. Van Duyne, in *Chemical and biochemical applications of lasers* (ed. Moore, C. B.) Vol. **4**, 101–184(Academic, New York, 1979).
28. K. A. Willets and R. P. Van Duyne, "Localized surface plasmon resonance spectroscopy and sensing," Annu. Rev. Phys. Chem. **58**(1), 267–297 (2007).

1. Introduction

When a metallic tip is exposed to an electromagnetic wave, the collective oscillating electrons known as surface plasmon polaritons (SPPs) lead to electric and magnetic fields that are confined to the metallic surface. The re-radiation of light at the same incident wavelength, referred to as plasmon scatter, is widely used in tip enhanced near field optical microscopy (TEONM) as nanosources for improved imaging spatial resolution and surface enhanced Raman scattering [1,2], or optical tweezers for manipulation of submicron particles and biomolecules [3].

For these applications, the metal tips are usually mounted to a metal-coated optical fiber probe on a shear-force-based scanning probe microscopy (SPM) for easy control of the position of the tip [1,4]. To create strong field enhancement at the tip apex, the electric field of the exciting laser beam should ideally be polarized along the tip's long axis [5]. The light guided by the optical fiber probe has been investigated to excite the SPPs of the metal nanorod attached to the probe tip [6,7]. Due to the extremely low throughout from the metal-coated fiber probe (10^{-4}-10^{-5}) [8], the efficiency with which SPPs are excited using this approach is limited. To overcome this, two other tip illumination methods are widely used. Non-transparent samples can be studied via side illumination by a single mode fiber (SMF) that delivers transverse polarized light. This transversely polarized light, delivered orthogonally to the tip, enables efficient excitation of SPPs at the tip apex of the metal particle attached to the fiber probe [9]. For transparent samples, on-axis illumination can be achieved using higher order laser modes. It provides access to strong longitudinal fields with field strengths comparable to their transverse components for tightly focused beams [10]. A major challenge of both of these illumination methods is that the external source field that is used to excite the metal tip also irradiates the sample directly. This direct irradiation of the sample leads to a background signal and limits the signal-to-noise ratio of the measurement. In addition, due to nano size of the metal particle, only a relatively small proportion of the energy of the excitation laser is coupled to the SPPs, leading to low excitation efficiency.

We propose that the illumination system could be greatly simplified by exciting the SPPs directly and efficiently via a new designed fiber probe itself. The removal of the external source also reduces the background signal associated with far-field radiation, and makes the

#145479 - $15.00 USD Received 6 Apr 2011; revised 6 Jun 2011; accepted 13 Jun 2011; published 28 Jun 2011

system portable, which enables particle manipulation with increased translation range or in areas that are difficult to access with traditional microscopy.

Here we explore the prospect of using a high index nano fiber probe without any metal coating to directly excite SPPs in metal nanorods located at the fiber's apex. The propagating modes of conventional silica optical fibers are well approximated by a Gaussian beam with a transversely polarized electric field. However, it has recently been recognised that the modes that propagate in the high index nanowires, or nanoscale core fibers, have significant electric field polarized along the propagation direction (the longitudinal direction) [11], and here we propose that this electric field can be used to excite SPPs of a metal particle located at the tip apex. The strength of the longitudinal field components of the nano fibers from high index lead silicate (F2 glass) and porous silicon, and the near field propagation from these fibers are investigated. The excitation of the SPPs at the end of the silver nanorods by the longitudinal field of these nanofibers is also explored numerically.

2. Non-transversality of the mode field

In order to develop novel fiber designs that can enable the efficient excitation of SPPs, the strength of the longitudinal component of the fiber mode field is first studied. High index glasses have been shown to enable enhancement of the relative contribution of the longitudinal component of the intensity [11]. The commercial F2 lead silicate glass from Schott Glass Co. (n=1.61 at λ=632nm) and silicon (n=3.54 at λ=1.1μm) were considered as potential host materials for the fibers. F2 glass has a low softening temperature (592 °C), which has led to the development of a broad range of microstructured fiber designs via the flexible extrusion technique for sensing and nonlinear applications [12–14]. Silicon represents the largest refractive index material fabricated into optical fibers to date [15].

A finite element method (FEM), based on the commercial package COMSOL Multiphysics, was used to study mode field distributions of the nano fibers. Three-dimensional Finite Difference Time Domain simulations (FDTD) from Lumerical Solutions were performed to investigate the propagation of the mode field in the near field and its excitation of SPPs in the silver nanorod. CST Microwave studio (MWS), a commercial 3D full vectorial simulation tool based on finite integration technique, was also used to confirm results obtained by the FDTD method. The wavelengths of excitation sources were selected to be at the edge of the absorption spectrum of the fiber materials to achieve the highest indices of the host glasses, and thus the largest longitudinal components in the guided modes. The excitation wavelengths are chosen to be 632nm for the F2 fiber and 1.1μm for the silicon fiber.

Fibers with core dimensions significantly larger than the wavelength of light have essentially transversely polarized guided modes. When the diameter of a fiber core is reduced, the longitudinal component starts to become significant [11]. The simplest structure is freestanding nano fibers, which have been considered here. Figure 1a shows intensity of both the transverse and longitudinal components of the mode field for silicon nano fibers with 300nm and 1.5μm diameters, respectively. Observe that the intensity $|E_z|^2$ of the longitudinal component is maximized at positions where the transverse spatial derivative is maximized, and that the largest $|E_z|^2$ amplitude occurs near the fiber interface. For linearly polarized field, the longitudinal component symmetrically distributes at both sides of the fiber core along the polarization direction as shown in Fig. 1a. From their corresponding cross-sectional profiles, it can be seen that both components are comparable in magnitude when the size of the silicon fiber is 300nm, while intensity amplitude of the longitudinal component $|E_z|^2$ is negligible when the core size is increased to 1.5μm diameter.

#145479 - $15.00 USD Received 6 Apr 2011; revised 6 Jun 2011; accepted 13 Jun 2011; published 28 Jun 2011

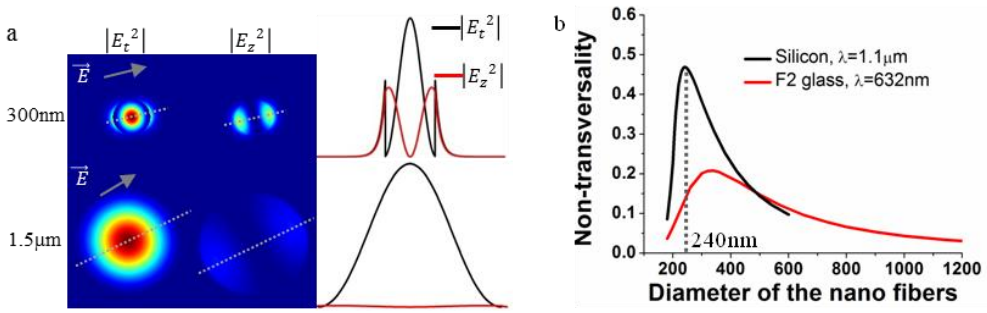

Fig. 1. (a). Intensity distribution of the transverse component E_t and longitudinal component E_z of the mode field for the silicon fibers with 300nm and 1.5μm diameter, respectively, and corresponding cross-sectional profiles taken along the dashed lines (the field is polarized along the dashed line). (b). Dependence of the non-transversality on fiber diameter for the F2 and silicon fibers.

To characterize the strength of the longitudinal component E_z relative to that of the total electric field $\vec{E}$, the non-transversality parameter $\int_\infty |E_z|^2 dA / \int_\infty |\vec{E}|^2 dA$ is defined as in Ref [11]. The dependence of the non-transversality on fiber diameter was calculated for the F2 glass at the wavelength of 632nm and silicon at 1.1μm and is shown in Fig. 1b. The non-transversality of the mode field approaches to zero in the regime of large core diameter, indicating the modes become essentially transverse as expected. With reduced fiber size, the magnitude of the longitudinal component increases, which leads to increased non-transversality. For the F2 fibers, the longitudinal component increases almost 5 times when its diameter is reduced from 1μm to 340nm. Unsurprisingly, the high index silicon fiber shows higher non-transversality in the limit of small cores, and its maximum non-transversality at the diameter of 240nm is 0.47, more than 2 times higher than that of the F2 glass fiber at the diameter of 340nm. Observe that with increased fiber size, the non-transversality of the silicon fibers reduces more quickly than that of the F2 fibers. To understand the impact of this non-transversality of the guided modes on the capacity of these fibers to serve as tools for microscopy and imaging, it is now important to understand how the longitudinal component of the field changes under propagation from the end of the fiber.

3. Non-transversality of the near field

In Section 2, the non-transversality of the mode field of the F2 glass and silicon fibers was explored. In this section we investigate light propagation in the near field, after the guided mode emerges from the fiber tip, and we explore the variation of the two components of the electric field as a function of the propagation distance using FDTD simulations. Figure 2a is a sketch of the geometrical arrangement for excitation of the mode field of a fiber located in vacuum environment. Cartesian coordinates with the origin located at the center of the output endface of the fiber are used, where the z axis is along the fiber axis. The FDTD computational domain is restricted to the area enclosed by the blue dashed lines. The propagation of the mode along a 2μm length of the fiber is shown, along with the propagation of light in the near field for a distance of 1.5μm outside of the fiber (from $z = 0$ to $z = -1.5$μm). The perfectly matched layeres (PMLs) are designed by Lumerical to absorb all incident light on them. The fundamental mode field of the fiber with unit amplitude is launched from the left, and is assumed to be x-polarized. The computational domain is discretized into a non-uniform orthogonal 3-dimensional mesh with a mesh size of 10nm for the fiber based on convergence testing. Before FDTD based on this setup is used for detailed calculations, as an example, the normalized amplitude of the field (to the amplitude of the

#145479 - $15.00 USD Received 6 Apr 2011; revised 6 Jun 2011; accepted 13 Jun 2011; published 28 Jun 2011

launch field) on the plane 50nm away from the fiber output endface for a 300nm silicon fiber has been modelled using FDTD and MWS, respectively. We have found that both values are within 4 significant figures ($|E_{max}|$=0.8534). The subsequent calculations are performed by FDTD, which is less computationally intensive.

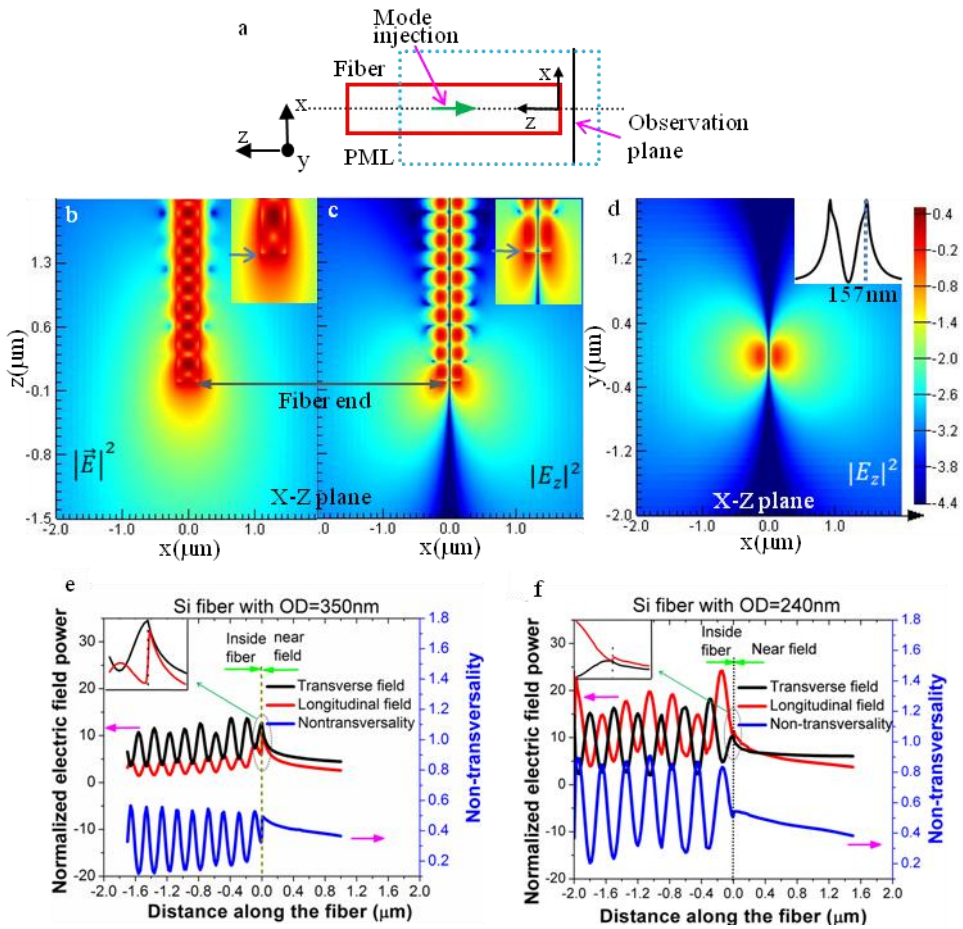

Fig. 2. (a). Configuration used to excite the fiber mode field (in vacuum). Excitation source is the fiber fundamental mode field polarized along x axis and injected along the fiber's z axis. (b) & (c). Propagation patterns of the total electric field and its longitudinal component (on a log scale) in the x-z plane (y=0), respectively, for the 350nm silicon fiber. Inserts are magnified field image around the fiber end. (d). Intensity distribution of the longitudinal field on the output endface (xy plane) of the same silicon fiber. Insert is the cross-sectional profile along the line y = 0. (e) & (f). Non-transversality and normalized power of the transverse and longitudinal components for the silicon fibers with their diameter as 350nm and 240nm, respectively. Insert magnifies the region around the fiber interface.

Figure 2b and 2c show the propagation patterns of the total electric field and its longitudinal component (on a log scale) in the x-z plane (y=0), respectively, for the 350nm silicon fiber, and Fig. 2d displays the intensity distribution of the longitudinal field at the output endface of the same fiber (xy plane with z=0). The power carried by all field components, both within the fiber, and as the light emerges from the fiber end, is shown in Fig. 2e. This power is calculated by integrating the intensity $|E_t|^2$ or $|E_z|^2$ across the xy plane and normalized to the power of the excitation electric field. It is clear that both components exhibit a standing wave of the same period within the fiber but with a π phase shift. In the

#145479 - $15.00 USD Received 6 Apr 2011; revised 6 Jun 2011; accepted 13 Jun 2011; published 28 Jun 2011

near field, both power values of the transverse field and longitudinal field decrease with increased propagation distance but the power of E_z reduces somewhat more quickly immediately outside the fiber endface, then does very similar to that of E_t. Therefore, the non-transversality oscillates at a magnitude of 0.6 inside the fiber, and slightly reduces with the propagation distance in the near field from an initial value of 0.5 at the endface of the fiber. Note that intensity of the longitudinal component $|E_z|^2$ is discontinuous at the output endface of the fiber as shown in inset of Fig. 2e (red curve). This is due to continuity of the electric displacement field at the air-fiber interface by Maxwell equations [16,17]. For convenient comparison, the power carried by all field components for the 240nm silicon fibers is also shown in Fig. 2f, which will be discussed later.

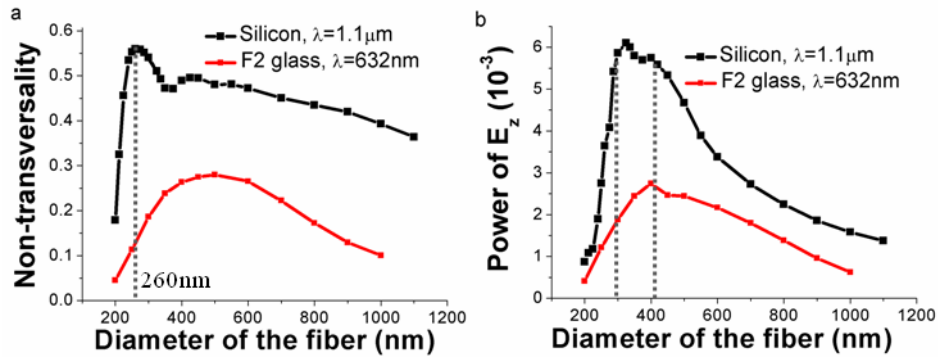

Fig. 3. Dependence of the non-transversality of the field in the near field on the diameter of the silicon and F2 fibers. (a). Non-transversality in the x-y plane 50nm away from the fiber output endface. (b). Power of the longitudinal component contained in a circle with 40nm diameter and centered at the point of its maximal intensity in the same plane as (a).

To explore ways of maximizing the non-transversality in the near field to enable highly efficient excitation, we explore the dependence of the non-transversality on diameter of the fibers, and values in the plane 50nm away from the endface of the fiber are shown in Fig. 3a (the reason of choosing 50nm is because the length of the silver rod for SPP generation used in Section 4 longer than 200nm). Comparing to Fig. 1b showing that the non-transversality of the fiber mode field, it can be seen that the non-transversality in the near field displays higher values than that in the mode field probably due to a significant jump in amplitude of the longitudinal field component at the endface of the fibers as shown in the insert of Fig. 2e. In the range of the large diameter (> 400nm) of the fibers, the near field non-transversality reduces far less with increased fiber diameter probably due to less jump amplitude for the smaller diameter fibers.

In order to test this hypothesis, the propagation of the field in a 240nm diameter silicon fiber is also modelled, and the power carried by all field components and their corresponding non-transversality along the fiber are shown in Fig. 2f. It can be seen from the insert that a discontinuity also exists in the power of the longitudinal field component at the output endface. However, this discontinuity is almost 5 times lower than that for the 350nm diameter silicon fiber. The reduced jump in amplitude for the smaller diameter fiber is partly caused by reduced confinement of the longitudinal field component inside the fiber core because the part of the longitudinal field distributed outside of the fiber is continuous at the plane formed by the fiber endface. If we define the core confinement of the longitudinal field as ratio of the power of E_z distributed in the core to the total power of E_z ($\int_{core}|E_z|^2 dA / \int_{\infty}|E_z|^2 dA$), it can be calculated using COMSOL that the core confinement of the 350nm diameter silicon fiber is two times more than that of the 240nm diameter silicon

#145479 - $15.00 USD Received 6 Apr 2011; revised 6 Jun 2011; accepted 13 Jun 2011; published 28 Jun 2011

fiber. This contributes to the increased strength of the longitudinal component in the near field for the larger diameter fibers.

The difference in core confinement alone is not sufficient to explain the factor of 5 times difference in amplitude discontinuity for the 240nm and 350nm diameter silicon fibers. In reality, the field propagation and reflection at the endface for these high index nano fibers are complicated. We have used an analytical method [17] to find the fiber modes for the silicon fibers and found that the maximum diameter for an air clad silicon fiber to guide a single mode is 240nm, which closely corresponds to the diameter at which the non-transversality is maximized, as shown in Fig. 1b. This means that higher order modes can propagate in the 350nm diameter silicon fibers. By using MWS, which is capable of predicting the behaviour of all the modes excited within the 3D devices, we have found that even when excitation is performed using the fundamental mode, higher modes are excited at the endface of this fiber upon reflection. In addition, using COMSOL we have shown that the radially polarized first order mode exhibits a strong longitudinal field component in the center of the silicon fiber core. This mode is usually referred to as the TM01 mode in conventional step-index fibers, which shows zero longitudinal component intensity at the center of fiber core. This mode may also contribute higher jump in amplitude for the 350nm diameter silicon fiber. A more complete analysis of the higher order mode excitation is beyond of the scope of this paper.

A higher non-transversality in the near field than their corresponding fiber mode field is helpful for improved excitation efficiency of the SPPs on the metal particles. However, for high resolution applications in imaging and nanolithography with SPP radiation, as demonstrated in Ref [2], the size of the metal particles is typically of order of tens of nanometers. When a single gold nanoparticle acts as nanosource, a 20 to 30nm spatial fluorescence resolution in fluorescence microscopy requires the diameter of a gold sphere below 100nm [2]. For effective excitation of SPPs within such a small particle, the energy distribution in a local area where the metal particle is located is more important than the whole power of the excitation source. Thus the spatial distribution of the propagated field from the fiber within the local area is more important than the total power in the whole plane. As shown in Fig. 2d, the power of the longitudinal component E_z in the output endface plane is concentrated near the edge of the fiber. For the 350nm diameter silicon fiber, the maximized longitudinal component intensity on the output endface is located at the x-axis with x = 157nm, and the $1/e^2$ width of the longitudinal field distribution is 260nm. Thus we calculate the normalized power of the longitudinal component E_z in a circle of area ($\int_{40nm}|E_z|^2 dA / \int_{\infty}|\vec{E}|^2 dA$) in the fiber endface plane as a function of the diameter of the fibers. The central point of the circle is located at the x axis, and has the maximum $|E_z|$ along the x axis. The diameter of the circle area is chosen as 40nm. This is because the SNOM is usually used for observation of the SPP excitation on the metal particles. The best resolution of the SNOM with an aperture is around 30-50nm. The power of the longitudinal component E_z in the local area as a function of the diameter of the fibers is shown in Fig. 3b. Now the difference in the non-transversality for the silicon fibers with different diameters becomes more apparent (compared with Fig. 3a). For diameters in the range 300nm to 400nm, the silicon fibers provide the strongest E_z energy in the circular area due to more concentrated longitudinal field. For the F2 fibers, although this difference is less significant, it can be still seen that a fiber with 400nm diameter can have the largest longitudinal component in the local area. With the same diameter of 400nm, the silicon fiber provides over 2 times higher field energy in this area. When a metal particle is located at the center of this circle area, the maximal SPPs may be excited, which will be discussed in the following section.

#145479 - $15.00 USD Received 6 Apr 2011; revised 6 Jun 2011; accepted 13 Jun 2011; published 28 Jun 2011

4. Excitation of the SPP mode of the silver nanorod

In this section, the excitation of the SPPs within a silver nanorod by the fibers is investigated. The shape of the silver nanorod is assumed to be that of a hemispherically-capped cylinder, which approximates fabricated nanorods [18]. The dielectric constants of silver are fitted by using bulk values reported by Palik [19]. The plasmon resonance for nanorods is known to split into two bands [20]. The short wavelength band corresponds to the oscillation of the electron perpendicular to the rod long axis described as transverse surface plasmon resonance (SPR). The other absorption band, which is red-shifted to long wavelengths, is caused by the oscillation of electrons along the rod's long axis (longitudinal SPR). As the aspect ratio (length L over diameter D of the rod) increases, the wavelength separation between the resonance wavelengths of the two plasmon bands increase. Thus the SPR resonant wavelength of the silver rod can be adjusted by changing its aspect ratio [18]. This ensures the longitudinal surface plasmon resonates at 1.1μm for the silicon fiber and 632nm for the F2 fiber. In Section 1, it is mentioned that the usual illumination method in TEONM is using standard SMFs. To compare the SPP excitation efficiency using the high index nano fibers, we first modelled excitation of the SPPs by standard SMFs, an approach that has been demonstrated experimentally, although no modelling results appear to have been reported. We do this as a means of providing a comparison with more advanced excitation approaches later in this paper (see Section 4.2). It is also noted that the field intensity shown in the results are normalized to unit intensity amplitude of the excitation source.

4.1 The SPPs of the silver nanorod excited by SMFs

The excitation source from the SMFs can be assumed to be a collimated Gaussian beam. The mode field diameter (MFD) of the Gaussian beam is dependent on the lens type, and a small MFD leads to higher excitation efficiency. Currently the minimum MFD of the collimated Gaussian beam achieved by commercial lensed fibers is around 50 μm [21], which is chosen in our modelling here. The SMF excitation efficiency calculated in this section represents the largest value possibly using external fiber excitation.

Figure 4a illustrates the setup used to excite SPPs using a collimated Gaussian beam. The FDTD computational domain is restricted to the area enclosed by the blue dashed lines. Cartesian coordinates with the origin located at the center of the long axis of the silver rod are used, where the z axis is along this long axis of the silver rod. The fiber axis is tilted as was used in practice in Ref [9]. Here the tilt angle of the fiber axis relative to y-axis is assumed to be 30 degrees. The observation plane is located 5nm away from the apex of the silver rod. When the localized SPP radiation is used as a nano source in scanning probe microscopy, 5 nm is the closest distance typically achieved between the source and sample surface using shear force feedback.

The diameter of the silver rod is fixed at 40nm. It is known that the plasmon resonance wavelength of the gold nanorod is near 900nm when its aspect ratio is equivalent to 4.2 [18]. By referring to this ratio, the length of the silver rod is scanned from the range of 200nm to 290nm to observe field intensity distribution on the observation plane. After convergence testing, the mesh size in the area including the silver rod is set as 1.5nm for accuracy. In order to save time, the computational domain is set as 2μm ×2μm ×2μm with the beam width kept as 50 μm. Figure 4b and 4c display electric field intensity distribution on the xz plane (y=0) and the observation plane (xy plane), respectively, at the wavelength of 853nm for a silver rod with an aspect ratio of 5 (L=200nm). It can be seen that the strongly localized field at both ends of the rod is observed due to excitation of the SPPs. Actually the wavelength of 853nm corresponds to longitudinal SPR [20] as shown in Fig. 4e, which shows spectral dependence of the maximum electric field intensity $\left|\vec{E}\right|^2$ on the observation plane. It can be seen that the strength of the localised field on the observation plane varies with wavelength.

#145479 - $15.00 USD Received 6 Apr 2011; revised 6 Jun 2011; accepted 13 Jun 2011; published 28 Jun 2011

The main broad peak at the wavelength of 853nm is produced due to longitudinal SPR, while the second smaller peak at the wavelength of 490nm comes from transverse SPR [20]. Due to most of the launch field polarised along the long axis of the silver rod, the longitudinal SPR scatters stronger field than the transverse SPR. It has been found that an aspect ratio of 7.25(L = 290nm) corresponds to the longitudinal SPR wavelength of 1.1μm.

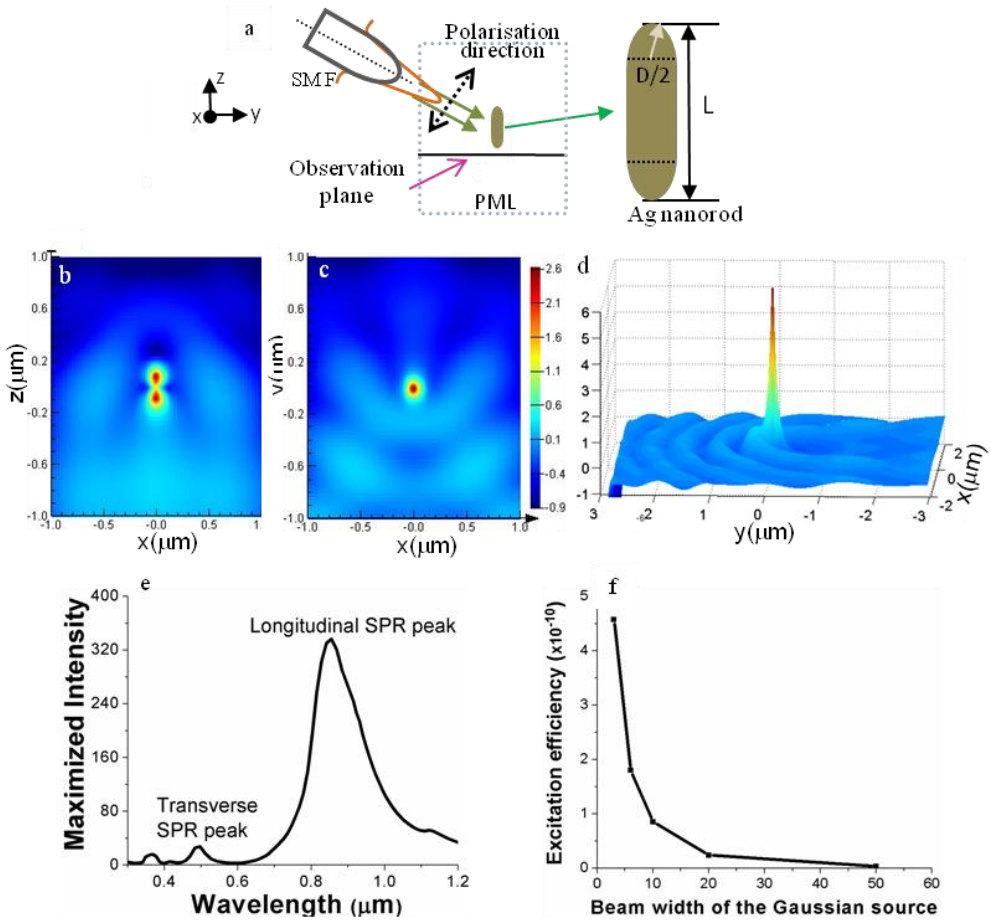

Fig. 4. (a) Geometrical arrangements for excitation of SPPs of the silver rod by collimated Gaussian beam from the SMF with a vacuum surrounding. (b)-(c) Electric field intensity distribution on the observe plane (xz plane) and the xy plane (z=0), respectively, for the silver rod with L=200nm at the wavelength of 853nm. (d) 3D electric field intensity distribution on the observe plane (xy plane) for the silver rod with L=290nm at the wavelength of 1.1 nm. (e) Spectral dependence of the maximized intensity of the longitudinal field on the observation plane for the silver rod with L=200nm. f. Excitation efficiency as a function of the beam width of the Gaussian source.

To investigate the strength of the SPR field excited by a Gaussian source with 50 μm beam width, the computational domain is increased to 80μm×80μm×6μm (the length of the cell along y axis is 6 μm). The aspect ratio of the silver rod is fixed at 7.25. Figure 4d quantifies electric field intensity distribution on the observe plane (xy plane) for this rod.

We use the excitation efficiency as a means of comparing the performance of different illumination systems. It is defined as ratio of the power of the scattered electric field from the SPR on the observation plane to the source power. The former is obtained by integrating the electric field intensity $\left|\vec{E}\right|^2$ on the observation plane over a circle area with its central point at

#145479 - $15.00 USD Received 6 Apr 2011; revised 6 Jun 2011; accepted 13 Jun 2011; published 28 Jun 2011

the z axis. For simplicity, the diameter of the circle area is chosen as $1/e^2$ width of the electric field on the observation plane, which is 66nm calculated from Fig. 4d. According to this definition, the excitation efficiency achieved using other Gaussian beams with different beam sizes was also calculated and shown in Fig. 4f. It can be seen that the excitation efficiency exponentially reduces with increased beam size. As mentioned previously, the excitation efficiency of $3.5\text{x}10^{-12}$ by the 50μm width Gaussian source represents the largest value that can be achieved using SMFs for far field illumination. A good approach to increasing the excitation efficiency is using smaller size beams, in particular near field illumination using the same SMFs. However, a simple reduction in the gap between the fiber endface and the silver rod in Fig. 4a is challenging due to difficulties in mounting the silver rod. Thus in the following section, the excitation of the SPPs on a silver rod vertically positioned on the endface of the nano fibers is simulated.

4.2 The SPPs of the silver nanorod excited by the silicon fiber

To simulate the excitation of SPPs by the nano fiber in the near field, the same setup system as in Fig. 2a is used with a silver nanorod introduced in the x axis as shown in Fig. 5a. The diameter of the silicon fiber is chosen to be 350nm, which corresponds to the maximized $|E_z|^2$ intensity in the near field as shown in Fig. 3b. A silver rod with 40nm diameter is first located at x=157nm where the maximum $|E_z|^2$ intensity exists on the output endface of the fiber. By changing the length of the silver rod during a series of calculations, it is found that the resonant plasmon wavelength of 1.1μm corresponds to a length of 204nm (L/D=5.1) which is shorter than the silver rod used in the far field excitation of the SMFs due to the different local refractive index around the rod.

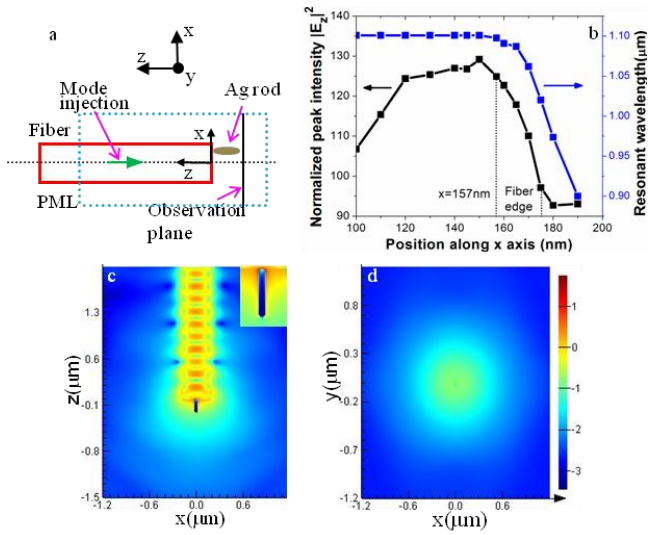

Fig. 5. (a). Configuration for exciting SPPs on a silver nanorod in vacuum by the nano fiber in the near field. (b). Dependence of resonant wavelength and peak intensity as a function of the location of the silver nanorod for the 350nm diameter silicon fiber along x axis. (c). Electric field distribution on the xz plane (y=0), and (d) on the observation plane with the 204nm long silver rod located at the center of the output endface of the fiber (on a log scale). The insert in c is the field in the vicinity of the silver rod (magnified).

With a fixed rod aspect ratio of L/D=5.1 we observe that both the amplitude of the maximum $\vec{E}$ field intensity on the observation plane and the corresponding plasmon resonance wavelength change slightly when the position of the rod shifts along x-axis. The

#145479 - $15.00 USD Received 6 Apr 2011; revised 6 Jun 2011; accepted 13 Jun 2011; published 28 Jun 2011

dependence of these parameters on the location of the silver rod along the x-axis is shown in Fig. 5b. In the range of 130nm to 150nm for the silver rod position, the SPR radiated field displays maximized resonant field at the wavelength of 1.1μm. When the silver rod is shifted to the center of the x axis, the results are phenomenologically different. Figure 5c and 5d shows that the intensity images of the electric field on the xz plane (y=0) and on the observe plane, respectively, in this case. The intensity at the apex of the rod approaches zero due to zero longitudinal component of the fiber mode field at this location of the silver rod (no SPP excitation along the long axis of the silver rod). It can be seen from Fig. 5b that a combination of the silver rod length of 204nm(L/D=5.1) and an edge position of 150nm along x axis produces the largest enhancement in the SPR field due to resonance occurring at the required wavelength of 1.1μm as indicated. At x=157nm, the normalized peak intensity has a slight reduction.

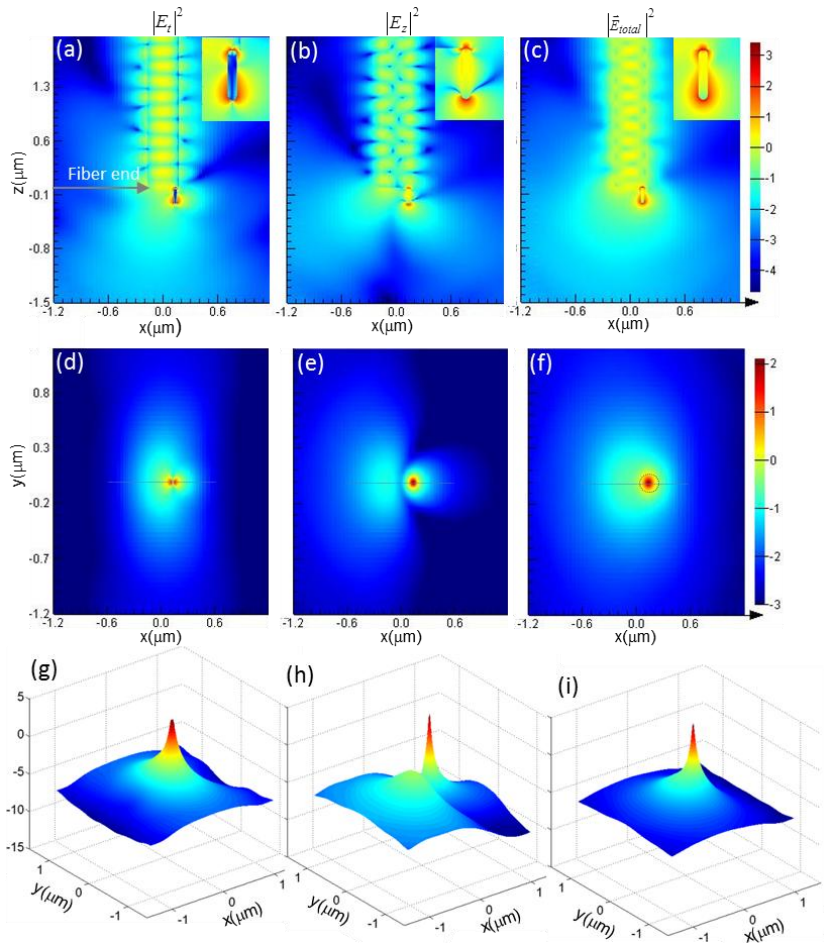

Fig. 6. Field intensity distribution (on a log scale) for the 350nm diameter silicon fiber and the silver nanorod (D=40nm, L=204nm) located at 140nm position on the x-axis. First column (a, d and g) is for the transverse component E_t. Second column (b, e and h) is for E_z. Third one (c, f and i) is for the total electric field $\vec{E}$. Images in the first row are from the x-z plane (y=0), the inserts show a close-up of the field distribution around the silver rod. Second row are from the observation plane, those from the third row are 3D plot for those from the second row. Inserts in (a) to (c) are magnified silver rod.

#145479 - $15.00 USD Received 6 Apr 2011; revised 6 Jun 2011; accepted 13 Jun 2011; published 28 Jun 2011

Figure 6 shows the images of the electric field intensity distribution under this condition. Columns 1, 2 and 3 correspond to the transverse component intensity $|E_t|^2$, the longitudinal component $|E_z|^2$ and the total electric field $|\vec{E}|^2$, respectively. Images in the first row (Fig. 6a to 6c) are from the xz plane (y-0), the second row (Fig. 6d-6f) are those on observation plane. The third row (Fig. 6g to 6i) quantifies the intensity distribution of the fields in Fig. 6d to 6f, respectively. From these images, it can be seen that strongly localized field are excited at the end of the silver rod due to excitation of the resonant plasmon, and the transverse field is only located at the edge of the silver rod as shown in the insert of Fig. 6a. If we compare Fig. 6i to Fig. 4d, it can be seen that for the excitation by the nano fibers, the fiber mode field including transverse component (Fig. 6d) and part of the longitudinal field at the right side (Fig. 6e) forms a source of background signal relative to the localised SPP field. For the excitation by the SMFs, the source field in the background (Fig. 4d) is relatively lower. The contrast is defined as $C = (|\vec{E}_{\max}|^2_{signal} - |\vec{E}_{\max}|^2_{background}) / |\vec{E}_{\max}|^2_{background}$, where $|\vec{E}_{\max}|^2_{signal}$ and $|\vec{E}_{\max}|^2_{background}$ are the maximised total electric field intensity and maximised background signal on the observation plane, respectively. For the electric field image that can be interpreted visually, its contrast needs to be larger than 1. The contrast for Fig. 6i is nearly 305 according to this definition, while it is 620 for the SMFs (Fig. 4d).

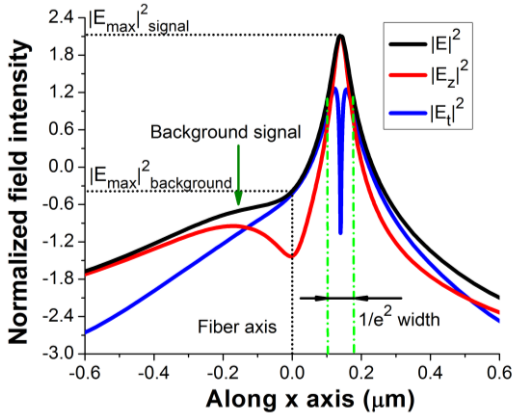

Fig. 7. Cross-sectional profiles of field intensities taken from Figs. 6d, 6e and 6f.

The cross-sectional profiles (along the x axis(y=0)) of Fig. 6d to 6f are plotted in Fig. 7. The $1/e^2$ width of the total field is 66nm, which is the same as that obtained by the SMFs excitation. Thus the beam size of the scattering field of the resonant plasmon is determined by the diameter of the silver nanorod. Thus it is easy to adjust aspect ratio of the silver rod for smaller $1/e^2$ width. Such a localised field is promising for use as a nano source for high-resolution imaging or photolithography.

For the calculations of the excitation efficiency performed here, the launched power is taken to be the power flowing out from the observation plane of the 350nm diameter fiber without the silver rod attached (Fig. 2a). The observation plane is chosen to be 5nm away from the fiber endface. Thus, as a result of the much more confined longitudinal field exhibited by the fiber mode field, the excitation efficiency by the 350nm diameter silicon fiber is 5.6×10^{-9}, about 1600 times higher than that by the SMFs.

#145479 - $15.00 USD Received 6 Apr 2011; revised 6 Jun 2011; accepted 13 Jun 2011; published 28 Jun 2011

4.3 The SPPs of the silver nanorod excited by the F2 fiber

Due to current availability of F2 suspended nano fibers with low loss [12], it is useful to also study plasmon excitation by the F2 fibers. Referring to Section 3, we set the diameter to be 400nm to maximise the longitudinal component in the near field. The diameter of the silver rod is still fixed at 40nm, and its length was optimised to match its plasmon resonant wavelength to 632nm. The optimum value for the silver rod length was found to be 130nm.

As for the silicon fiber, the electric field intensity distributions are calculated (see Fig. 8). They are similar to the silicon results shown in Fig. 6. The cross sectional profiles (along x axis) of Fig. 8d to 8f are plotted in Fig. 9. Relative to the images to Fig. 7, it can be seen that due to smaller non-transversality of the F2 fiber than the silicon fiber, the electric field on the observe plane displays stronger background signal. The contrast in Fig. 8f is 37 times based on Fig. 9, which is 1.85 times lower than Fig. 6f for the 350nm diameter silicon fiber. A reduced contrast (1.85 times lower) compared to excitation by the 350nm diameter silicon fiber indicates that it is harder to detect the localised SPR field in F2 fibers using tools such as SNOM.

Due to the same diameter of the silver rod used, the $1/e^2$ width of the total field shows very similar value as that in the silicon fiber and is about 63nm. The excitation efficiency by the 400nm diameter F2 fiber is calculated as 2.3×10^{-9}, about 2.5 times lower than that of the 350nm diameter silicon fiber.

By comparing the results obtained using three illumination methods for excitation of SPR on the silver rod, it is clear that the excitation efficiency achieved by the 350nm diameter silicon nano fiber is almost three orders of magnitude higher compared to the more traditional SMF excitation. As mentioned in Section 4.2 and shown in Fig. 6d-6f (also Fig. 8d-8f in Section 4.3), due to effect of the transverse component of the mode field, the contrast of the SPR field image excited by the silicon or F2 fiber is lower than that achieved by the SMFs. With the high index nano fibers, index contrast of the fibers plays a major role in the control of the excitation of the SPR in the metal particles. A higher index contrast leads to higher image contrast for detection, in addition to higher excitation efficiency.

#145479 - $15.00 USD Received 6 Apr 2011; revised 6 Jun 2011; accepted 13 Jun 2011; published 28 Jun 2011

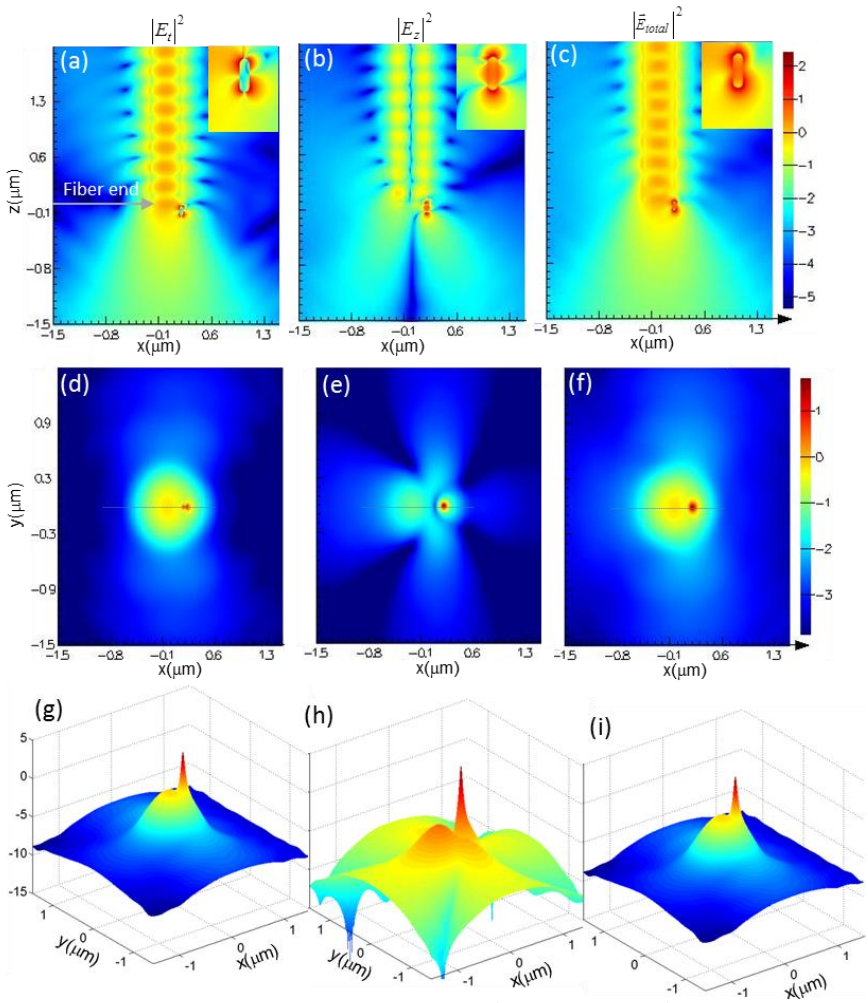

Fig. 8. Field intensity distribution (on a log value) for the 400nm F2 fiber and the silver nanorod located at its output endface. The first column (a, d and g) is for the transverse component E_t, the second column (b, e and h) is for E_z, the third one (c, f and i) is for the total electric field $\vec{E}$. The pattern images in the first row are from the x-z plane (y=0), those in the second row are from the observation plane (xy plane), those from the third row are 3D plot for those from the second row.

#145479 - $15.00 USD Received 6 Apr 2011; revised 6 Jun 2011; accepted 13 Jun 2011; published 28 Jun 2011

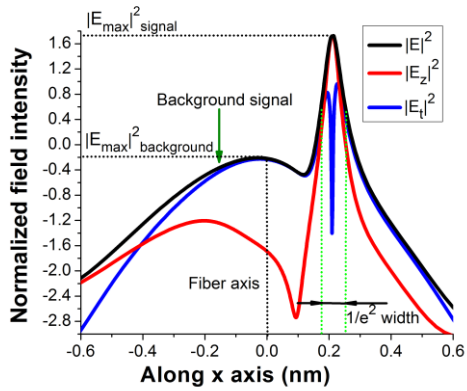

Fig. 9. Cross sectional profile of Fig. 8d,8e and 8f along x axis when the silver rod is excited by a F2 nanofiber.

5. Discussions and conclusion

It has been theoretically demonstrated that the high index nano fibers can be used to excite longitudinal SPR within metal nanoparticles attached to their output end by exploiting the fiber's strong longitudinal field component. A silver rod with a diameter fixed at 40nm was chosen for plasmon excitation. The aspect ratio of this rod can be adjusted to match the plasmon resonance wavelength of the rod to that of the light propagating in the fibers. Strongly localised fields excited by a 350nm diameter silicon fiber or 400nm F2 fiber have been demonstrated.

Field excitation efficiency by the 350nm silicon fiber is three order higher than that by the SMFs at the wavelength of 1.1μm. The 400nm lower index F2 fiber provides relatively lower excitation efficiency and contrast of the SPR radiation due to smaller index contrast of the fiber. Due to the same diameter of the silver rod used, the SPR radaited electric fields excited by both fibers presents similar $1/e^2$ width, and is around 63-66nm.

The next step is to perform experimental characterisation of the longitudinal field from these high index fibers and explore their capacity to excite SPPs within metal particles. Single fluorescent molecule can be used to probe longitudinal field component because the absorption dipole moment of a molecule maps the spatial distribution of the intensity of exciting electric field polarised along its dipole direction [22,23]. For observation of longitudinal SPR field, an array of the silver nanorod [24] can be excited by our high index nano fibers at the wavelength corresponding to the longitudinal SPR peak, and its scattered SPR field is collected using SNOM system. The metal nano rod vertically positioned on the endface of the nanofibers displays different scattering strength with different position as discussed in Section 4.2. By scanning the surface of the silver nanorod array opposite to the incident plane, the field intensity distribution on this surface can be collected by the fiber probe, which can be chosen to be cut-off at the wavelength corresponding to the transverse SPR peak. Therefore, the collected field intensity distribution is mainly caused by the SPR radiated field which is excited by the longitudinal component of the fiber mode field. By translating the nanorod across the fiber endface, one can map out the distribution of the intensity of the longitudinal field in the transverse plane. The transverse component of the mode field has been absorbed by the silver rod array to generate the transverse SPR, which has been filtered away by the fiber probe itself.

Although the high index nano fibers show a greater capacity for higher efficiency excitation of the metal nanorods than SMFs, the coupling loss from other sources to the nano fibers is expected to be relatively high due to small core size of the nanofibers. It can be compensated for by considering alternative fiber designs, either using enlarged fiber core to

#145479 - $15.00 USD Received 6 Apr 2011; revised 6 Jun 2011; accepted 13 Jun 2011; published 28 Jun 2011

reduce coupling loss or applying the first higher order mode of the nano scale fibers. For example, the radially polarized beams in the first higher order modes have been demonstrated to be generated and stably guided by the vortex fibers with a strong outer ring in the refractive index profile [25]. It has been shown that the radially polarised beams have a strong longitudinal field component in the central position of the beam [22] when they are strongly focused. As mentioned in Section 3, high index nano fibers may have much stronger longitudinal component for their first order mode polarised radially even without focusing. By manipulating structures of the high index soft glass fibers, the new fibers with highly confined longitudinal field should enable higher excitation efficiency of SPR with their contrast comparable to that of the SMFs [25].

The scattered SPR field from the metal particles provide an ideal nano source for high-resolution imaging and lithography [1,2,4]. When molecules adsorb onto the plasmonic metal particle or move to within a few nanometers of its surface, the localised electromagnetic field around the nano particle can enhance the Raman scattering by a factor of 10^{14}-10^{15} for single molecules [26], or fluorescence up to 30 times [2]. Thus the surface-enhanced Raman scattering results in a highly specific and sensitive method for molecular identification or detection [27]. These plasmonic nano particles also act as transducers that convert small changes in the local refractive index into spectral shift in the intense nano particle extinction and scattering spectra. Molecular binding can be monitored in real time with high sensitivity by using simple and inexpensive transmission spectrometry [28]. The strongly localised field around the plasmonic nano particle also enhance the optical force on objects [3]. Experimental data have provided a force magnitude enhancement factor of about 40 that could be attributed to the plasmon resonance [3]. The SPR field excited directly by the optical nano fibers makes the system portable, which enables these applications operating with increased spatial range or in areas that are difficult to access using traditional approaches. Such fiber-based sensing architectures are particularly promising for in-vivo label-free sensing applications due to their small size.

Acknowledgments

We acknowledge the Australian Research Council (ARC) for funding this project (DP0880436). Y. Ruan acknowledges the support of an ARC Australian Postdoctoral Fellowship, and T. Monro acknowledges the support of an ARC Federation Fellowship.

#145479 - $15.00 USD Received 6 Apr 2011; revised 6 Jun 2011; accepted 13 Jun 2011; published 28 Jun 2011